Medjunarodni naučno-stručni skup
XXV NAUKA I MOTORNA VOZILA SCIENCE AND MOTOR VEHICLES 2015
International Automotive Conference
14 - 15 April 2015, Beograd, Serbia

NMV15ASim02

FLAME TRACKING – PARTICLE METHOD FOR 3D SIMULATION OF NORMAL AND ABNORMAL (KNOCKING) OPERATION OF SPARK-IGNITION AUTOMOTIVE ENGINES

Frolov S. M., Ivanov V. S., Basevich V. Ya., Belyaev A. A.
Department of Combustion and Explosion, Semenov Institute of Chemical Physics, Moscow, RUS
Basara B., Priesching P., Suffa M.
Advanced Simulation Technologies, AVL List GmbH, Graz, AUT

ABSTRACT

The objective of the research outlined in this article was to upgrade the Flame Tracking – Particle (FTP) combustion model developed by the authors earlier and to apply it for predicting normal and abnormal (knocking) operation of spark-ignition internal combustion (IC) engines using AVL FIRE platform. Based on 3D simulations of multiple engine test cases a new correlation for the turbulent flame velocity has been suggested which provides reasonable predictions for engine pressure curves without tuning. Application of two-stage fuel oxidation kinetics allows the intensity of preflame reactions to be continuously monitored and the conditions for knocking combustion to be identified in terms of various statistics.

KEYWORDS: Internal combustion engine, normal and knocking operation, 3D simulation, Flame Tracking – Particle method.

INTRODUCTION

Multidimensional CFD has become an integral part of the design technology and refinement of IC engines. In view of it, the demands to the adequacy and predictive capability of models describing various physicochemical processes in the engine cylinder as well as to the accuracy of calculations are steadily increasing. The Institute of Chemical Physics of the Russian Academy of Sciences has long been cooperating with AVL LIST GmbH in developing, testing and implementing physical and mathematical models for AVL FIRE, the engine-oriented computer code for 3D simulation of the operation process in piston engines [1]. The objective of the joint research outlined in this article was to upgrade the FTP combustion model developed by the authors earlier [2] and to apply it for predicting normal and abnormal (knocking) operation of spark-ignition IC engines using AVL FIRE. Unlike other existing models of turbulent combustion, the FTP model considers chemical reactions both in the flame and in the volume and accounts for the principal difference between those: flame reactions proceed in the presence of thermal and diffusion fluxes whereas volumetric reactions proceed in the absence of such fluxes. The FTP model has been used previously for calculating combustion in confined spaces [2] and for calculating deflagration-to-detonation transition in gas explosive mixtures [3].

FLAME TRACKING METHOD

Formulation

The essence of the Flame Tracking (FT) method can be readily explained on the example of laminar flame propagation [2]. The flame surface shape and area are found based on the Huygens principle: Each elementary portion of the flame surface displaces in time due to burning of the fresh mixture at local velocity u_n (normal to the flame surface) and due to convective motion of the mixture at local velocity V. The local instantaneous velocity u_n is taken from look-up tables including in general the effects of mixture dilution with combustion products (exhaust gas recirculation), flame stretching, and flammability limits. The local instantaneous velocity V is calculated using a high-order interpolation technique. In 2D flow approximation, the flame surface is represented by straight-line segments, whereas in 3D calculations, the flame surface is represented by connected triangles.

In the turbulent flow field, a pulsating velocity vector distorts the “mean” reactive (flame) surface by wrinkling it. The local instantaneous flame wrinkling can be taken into account by proper increasing the normal flame velocity, or in other words, by introducing a local turbulent flame velocity $u_t = u_n S / S_n$, where S is the surface area of the wrinkled flame at a given segment, and S_n is the surface area of the equivalent “planar” flame segment. The problem now is to find the way of calculating u_t. In the theory of turbulent combustion, there are many correlations between u_t and u_n of the form $u_t / u_n = F(u', \nu, l, \delta, Le)$ [4–11], where u' is the local turbulence intensity, ν is the kinematic viscosity of combustible mixture, l is the integral length scale of turbulence, δ is the laminar flame thickness, and *Le* is the Lewis number.

Table 1 presents 8 different correlations (1 to 8) taken from the literature. Our calculations showed that Guelder correlation (#4 in Table 1) exhibits reasonable performance when applied to IC engines despite a need in certain tuning for obtaining the best fit between calculated and measured engine pressure curve.

Table 1: Correlations for turbulent flame velocity

No.	Correlation	Reference
1	$F = 1 + \frac{u'}{u_n}$	Damkoehler [4]
2	$F = \left(1 + \frac{u'^2}{u_n^2}\right)^{1/2}$	Shchelkin [5]
3	$F = 1 + 0.52\left(\frac{u'}{u_n}\right)^{1/2}\left(\frac{u'l}{\nu}\right)^{1/4}$	Zimont [6]
4	$F = 1 + 0.62\left(\frac{u'}{u_n}\right)^{1/2}\left(\frac{u_n l}{\nu}\right)^{1/4}$	Guelder [7]
5	$F = 1 + 0.95 Le^{-1}\left(\frac{u'}{u_n}\right)^{0.5}\left(\frac{l}{\delta}\right)^{0.5}$	Bradley [8]
6	$F = 1 + 0.435\left(\frac{u'}{u_n}\right)^{0.4}\left(\frac{u_n l}{\nu}\right)^{0.44}$	Liu et al. [9]
7	$F = -0.274\left(1 + \frac{u_n l}{\nu}\right) + \left(0.076\left(1 + \frac{u_n l}{\nu}\right)^2 + 0.547\left(1 + \frac{u_n l}{\nu}\right)\frac{u'}{u_n} + 1.547\right)^{0.5}$	Peters [10]
8	$u_t = u_n \exp(u'^2 / u_t^2)$	Yakhot [11]
9	$F = -4.37 + 1.13\left(\frac{u'}{u_n}\right)^{1/2}\left(\frac{u_n l}{\nu}\right)^{1/4}$ $\quad if\ F < 1 : F = 1$	Engine (this work)

Application to engines

To derive a proper correlation $u_t / u_n = F(u', \nu, l, \delta, Le)$ for IC engine conditions we checked the relevance of Guelder correlation to multiple engine test cases. For this purpose, we related u_t / u_n ***at the ignition point*** to the parameter appearing in the right-hand side of Guelder correlation $(u'/u_n)^{1/2}(l/\delta)^{1/4}$, provided that the predicted engine pressure curve fits well the experimental curve, i.e., we plotted the best-fit points on the plane

$$\frac{u_t}{u_n} \quad vs \quad \left(\frac{u'}{u_n}\right)^{1/2}\left(\frac{l}{\delta}\right)^{1/4}$$

It is implied that, if Guelder correlation is relevant to an engine test case, than the slope of the straight line approximating the best-fit points would be 0.62. As a matter of fact the black line in Fig. 1 corresponding to this slope does not in general fit the values u_t / u_n (at the ignition point) required for the best fit of predicted and measured pressure curves. It is seen from Fig. 1 that the red line fits the best-fit points much better. The red line from now on referred to as the "Engine correlation" corresponds to the following formula:

$$\frac{u_t}{u_n} = -4.37 + 1.13\alpha\left(\frac{u'}{u_n}\right)^{1/2}\left(\frac{u_n l}{\nu}\right)^{1/4} \qquad (1)$$

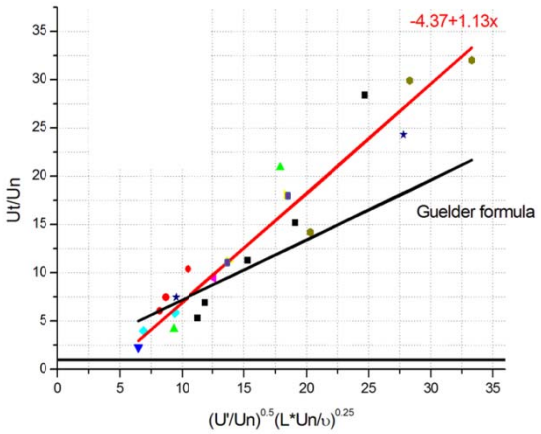

Figure 1: Engine test cases (points) and correlations for u_t / u_n : black line = Guelder correlation; red line = Engine correlation of Eq. (1).

where α is the fitting parameter with the default value of 1.0. Thus, the Engine correlation supplements the list of u_t / u_n correlations of Table 1 (#9) and is based on processing multiple IC engine test cases. Since the Engine correlation allows for the negative value of u_t / u_n, we put the physical constraint to it: if F<1 then F = 1. The scatter of points in Fig. 1 can be (at least partly) explained by the cycle-to-cycle variation of engine pressure.

To check the performance of the Engine correlation of Eq. (1), we have performed a number of calculations for different test cases. It appeared that this correlation provides satisfactory agreement with measured pressure curves for different engines at different load points. Consider Fig. 2 as an example of one automotive engine operating at four different load conditions OP1, OP3, OP4, and OP6. For all load conditions, α = 0.9.

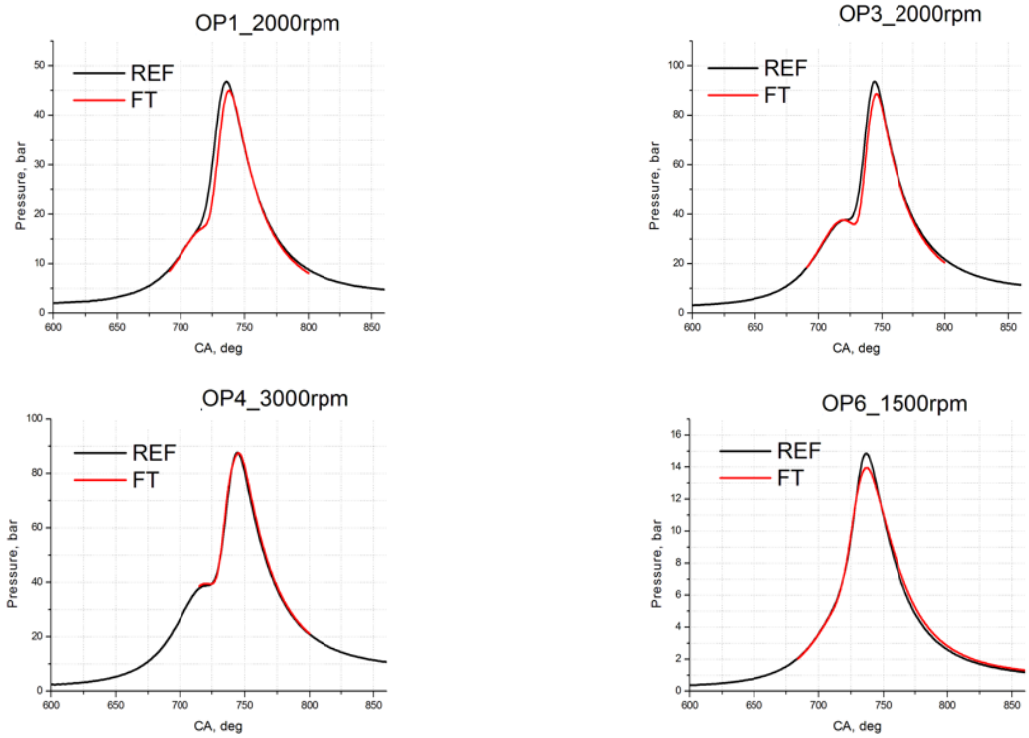

Figure 2: Comparison of predicted (red) and measured (black) pressure curves for different load points of one automotive engine with α = 0.9 in Eq. (1).

PARTICLE METHOD

Formulation

The preflame zone exhibits volumetric reactions of fuel oxidation, formation of intermediate products like alcohols, aldehydes, peroxides, etc. In general, preflame reactions are spatially nonuniform due to nonuniform distributions of temperature and main species concentrations and due to high sensitivity of reaction rates to these parameters. Therefore, preflame reactions can result in localized energy release.

Direct (and CPU time consuming) way to calculate volumetric reaction rates is to solve the equations of chemical kinetics in the preflame zone in each computational cell. To shorten the CPU time, we introduce a certain number of notional Lagrangian particles, which move in the preflame zone according to the local velocity vector [2, 12]. In each particle, preflame reactions proceed at the rates determined by its instantaneous temperature and species concentrations. For determining the time and location of preflame autoignition, a certain autoignition criterion is adopted. The criterion is based on the fixed rate of temperature rise in the particle, e.g., 10^6 or 10^7 K/s.

The mean (over all particles in cell) reaction rate directly affects the mean flow pattern. When the autoignition criterion is met in one or several particles, new (forced) ignition sites in the preflame zone are automatically introduced. In general, these ignition sites give birth to new laminar/turbulent flame kernels or, if the preflame reactions are fast, they result in the induction (spontaneous) flames and volumetric combustion. For keeping the number of particles at a reasonable level, the consistent procedures of particle cloning and clustering are developed. The preflame particles are traced until the entire geometry is traversed by the frontal or volumetric combustion.

In each *i*th Lagrangian particle, the following set of equations is solved:

$$\frac{dx_k^i}{dt} = u_k^i$$

$$\frac{d(\rho_l^i V^i)}{dt} = \nabla J_l^i + J_l^i \tag{2}$$

$$\rho^i \frac{du_k^i}{dt} = \frac{\partial P^i}{\partial x_k} - \nabla(Ep^i + \tau^i) \tag{3}$$

$$\rho^i \frac{dh^i}{dt} = -\nabla q^i + h_{\text{hom}}^i + \frac{\partial P^i}{\partial t} - P\frac{\partial u_k^i}{\partial x_k} \tag{4}$$

where x_k^i is the coordinate (k = 1, 2, and 3) and u_k^i is the velocity component, ρ_l^i is the partial density of the lth species, ρ^i is the mean particle density, V^i is the particle volume, ∇J_l^i is the diffusion flux of the lth species to/from the particle, and J_l^i is the flux of the lth species due to chemical reaction, P^i is the mean pressure, p^i is the pulsating pressure, E is the unit tensor, and τ^i is the molecular viscous stress, h^i is the particle enthalpy, q^i is the heat flux to/from the particle, h_{hom}^i is the heat effect of chemical reaction, $\partial P^i / \partial t$ is particle heating due to adiabatic compression, and $P\partial u_k^i / \partial x_k$ is particle heating due to shock compression.

Molecular diffusion term ∇J_l^i in Eq. (2), molecular heat transfer term ∇q^i in Eq. (4) and term $\partial p^i / \partial x_k + \nabla\tau$ in Eq. (3) are modeled using classical models of Interaction by Exchange with the Mean [12]:

$$\nabla J_l^i = -0{,}5C_1(Y_l^i - \overline{Y}_l^i)\rho^i V^i \omega$$

$$\nabla q^i = -0{,}5C_2(h^i - \overline{h}^i)\rho^i \omega$$

$$(\rho^i)^{-1}\nabla(p^i E - \tau^i) = -\zeta(u_k^i - \overline{u}_k^i) + A(t)$$

where C_1 and C_2 are the coefficients ($C_1 \approx C_2 \approx 2{,}0$), Y_l^i is the concentration of the lth species, $\overline{Y}_l^i$ is the mean concentration of the lth species at the location of the ith particle, ω is the turbulent frequency, h^i is the enthalpy, $\overline{h}^i$ is the mean enthalpy at the location of the ith particle, $\overline{u}_k^i$ is the mean kth velocity component at the location of the ith particle, ζ is the coefficient ($\zeta \approx 2{,}075\omega$), and $A(t)$ is the stochastic function in the Langevin equation.

Application to engines

The reaction mechanism of hydrocarbon fuel (gasoline) oxidation in the preflame zone used in the Particle method contains two stages: cool flame and hot explosion. The cool-flame stage is activated at low temperature and ends at a fixed temperature denoted as T^* (~920 K for gasoline). At temperature $T > T^*$, the cool-flame reaction is replaced with the hot-explosion reaction. At low temperatures $T < T^*$, the rate of cool-flame reactions is known to be higher than the rate of hot-explosion reactions in the preflame zone.

Figure 3 shows the predicted time histories of the cumulative progress variable of preflame reactions for three load points OP3, OP5, and OP6 of the same automotive engine as in Fig. 2. As seen, the highest value of the progress variable corresponds to load point OP3, whereas load point OP6 exhibits the lowest value of the progress variable. Since preflame reactivity is closely connected to knocking combustion, the highest and lowest knock probability should be attributed to load points OP3 and OP6, respectively. These predictions correspond well with experimental observations: load points OP3 and OP5 are in the region with relatively high knock probability, whereas load point OP6 is in the region with low knock probability. In general, knock probability is known to be higher for operation points with lower engine rotation speeds (RPM) and higher engine loads. Point OP5 exhibiting high load and high RPM possesses a lower knock probability than point OP3 due to a shorter time available for the preflame reactions to proceed before the turbulent flame traverses the combustion chamber.

Figure 4 shows the predicted time histories of the rate of energy release in the preflame zone for the same three load points. The rate of energy release in points OP3 and OP5 are nearly the same, whereas point OP6 exhibits the rate of energy release in the preflame zone two orders of magnitude lower.

It is worth to compare the contribution of cool-flame and hot-explosion energy release in the preflame zone. Figure 5 presents predicted time histories of such contributions for engine load point OP5. The dashed green curve shows the time history of the mass fraction of the preflame gas with temperature $T > T^*$, i.e. the preflame gas exhibiting the hot-explosion reaction stage. This means that the rest of preflame gas mass fraction has temperature $T < T^*$. It is seen that at crank angles less than 726 deg. the preflame zone is mostly occupied by the gas with cool-flame reactions, whereas at crank angles higher than 728 deg. the preflame zone is mostly occupied by the gas with hot-explosion reactions. The blue and red curves in Fig. 5 correspond to the cool-flame and hot-explosion energy release rates in particles with $T < T^*$ and $T > T^*$, respectively. Clearly, the rate of energy release in particles with $T < T^*$ (blue curve) is considerably higher than that in particles with $T > T^*$ (red curve).

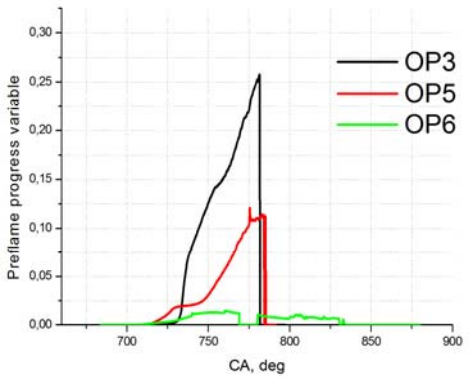

Figure 3: Predicted time histories of preflame reaction progress for three engine load points: OP3, OP5, and OP6.

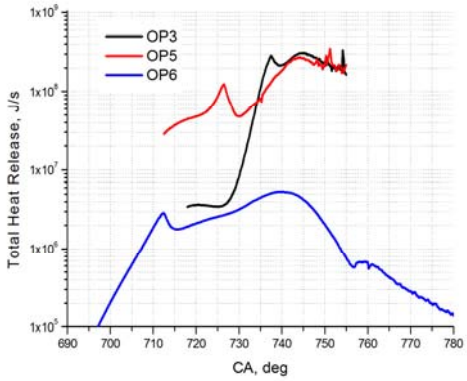

Figure 4: Predicted time histories of the rate of energy release in the preflame zone for three engine load points: OP3, OP5, and OP6.

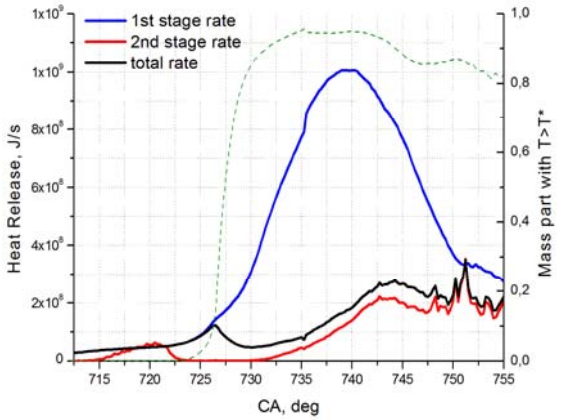

Figure 5: Predicted time histories of heat release due to cool-flame and hot-explosion reactions in the preflame zone for engine load point OP5. The dashed green curve shows the time history of the mass fraction of the preflame gas with temperature $T > T^*$, i.e. the preflame gas exhibiting the hot-explosion reaction stage.

The black curve in Fig. 5 shows the overall rate of energy release obtained as a sum of cool-flame and hot-explosion reaction rates normalized by the corresponding mass fractions. It appears that the contribution of cool-flame energy release is dominating at crank angles up to about 732 deg. At higher crank angles the hot-explosion reactions start contributing (compare red and black curves) but the contribution of cool-flame reactions is still considerable up to about 750 deg. CA.

The Particle method allows collecting diverse statistical information on the probability density functions (PDFs) of temperature, mixture composition, reaction progress, etc. all throughout the preflame zone or in its parts. As an example, Fig. 6 shows the predicted PDFs of fuel mass fraction and temperature for a certain part of the combustion chamber. Analysis of such plots allows conclusions to be made on the knock probability.

The simultaneous use of both Flame Tracking and Particle methods allows direct simulation of engine operation at knocking conditions with spatial and temporal resolution of preflame exothermic centers, explosions, and shock waves traversing the engine cylinder. In addition, such simulations allow estimating the contribution of preflame reactions to the pressure history in the engine. As an example, Fig. 7 compares pressure histories obtained for three engine load points OP3, OP5, and OP6 with and without activation of Particle method. As could be expected, at normal operation conditions (far from the knock) the contribution of preflame reactions is insignificant (compare red and blue curves for OP6) whereas at the operation conditions close to knock (compare red and blue curves for OP3 and OP5) some visible differences appear in the pressure curves, in particular, in terms of higher pressure peaks.

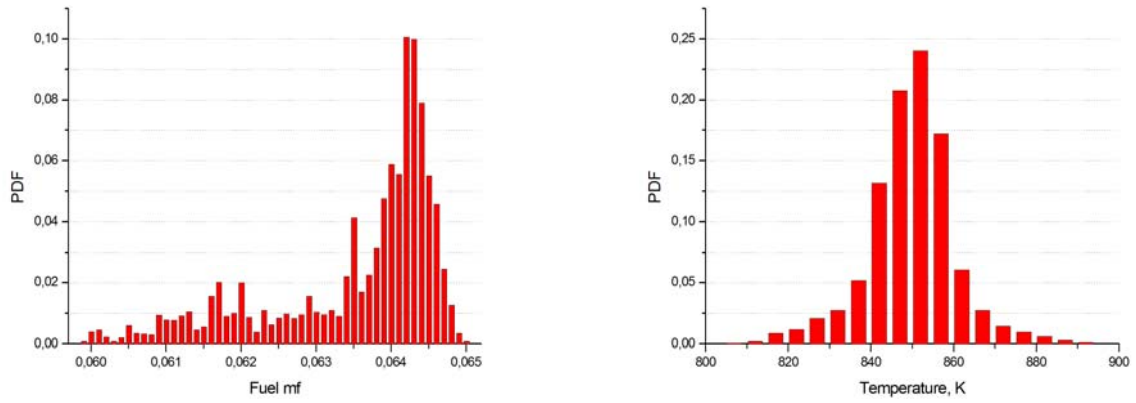

(a) (b)

Figure 6: Predicted probability density functions of fuel mass fraction (a) and temperature (b) for a certain part of the engine combustion chamber.

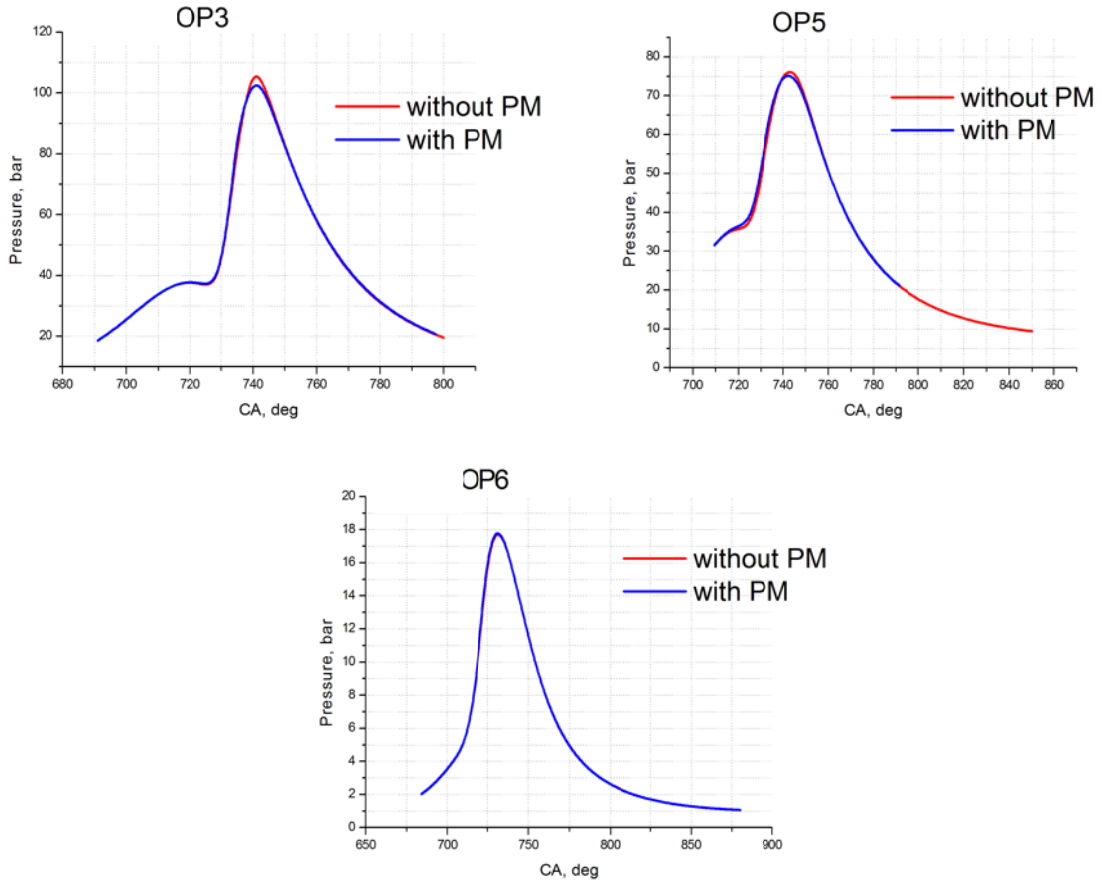

Figure 7: Comparison of predicted pressure histories obtained for three engine load points OP3, OP5, and OP6 with (blue) and without (red) activation of Particle method.

CONCLUSIONS

The FTP combustion model has been upgraded with the new correlation for the turbulent flame velocity applicable to various IC engines and with the procedures for the identification of knocking operation conditions. The new combustion model has been implemented into AVL FIRE platform and validated against experimental test cases. The FT method supplemented with the new correlation for the turbulent flame velocity ("Engine correlation") is shown to provide satisfactory agreement with measured pressure curves for different engines at different load points. The Particle method allows direct simulation of engine operation at knocking conditions with spatial and temporal resolution of preflame exothermic centers, explosions, and shock waves traversing the engine cylinder. In addition, it allows collecting diverse statistical information on the PDFs of temperature, mixture composition, reaction progress, etc. all throughout the preflame zone or in its parts.

ACKNOWLEDGMENTS

The support of this work by AVL LIST GmbH is gratefully acknowledged.

REFERENCES

1. AVL FIRE® - Computational Fluid Dynamics for Conventional and Alternative Powertrain Development: https://www.avl.com/fire.
2. Frolov S.M., Ivanov V.S., Basara B, Suffa M. Numerical simulation of flame propagation and localized preflame autoignition in enclosures. Journal of Loss Prevention in the Process Industries, 2013; 26: 302-309

3. Frolov S.M., Ivanov V. S. Numerical simulation of deflagration-to-detonation transition by coupled flame tracking - particle method. In: Progress in Propulsion Physics. Eds. L. DeLuca, C. Bonnal, O. Haidn, and S. Frolov. EUCASS Advances in Aerospace Sciences Book Ser. EDP Sciences, TORUS PRESS, 2011, Vol. 2, pp. 533-554.
4. Damkoehler G. Der einfuss der turbulenz auf die flammengeschwindigkeit in gasgemischen. Zs Electrochemie 1940; 6: 601–52.
5. Shchelkin K.I. Fast Combustion and Spin Detonation of Gases. Moscow: Voenizd; 1949.
6. Zimont V.L. Theory of turbulent combustion of a homogeneous fuel mixture at high Reynolds numbers. Combustion, Explosion, Shock Waves 1979; 15(3): 305-311.
7. Guelder Ö.L. Turbulent premixed flame propagation models for different combustion engines. Proc. Comb. Inst. 1990; 23: 743-750.
8. Bradley D. How fast can we burn? Proc Combust Inst 1992; 24: 247–53.
9. Liu Y., Ziegler M., Lenze B. Proc. Joint Meeting of the British - German Sections of the Combustion Institute, Cambridge (UK), 1993, pp. 64-67.
10. Peters N. The turbulent burning velocity for large scale and small scale turbulence. J. Fluid Mechanics 1999; 384: 107-132.
11. Ronney P.D., Yakhot V. Flame broadening effects on premixed turbulent flame speed. Comb. Sci. Techn., 1992, Vol. 86, pp. 31-43.
12. Pope, S.B., 1985, “PDF Methods for turbulent reactive flows”, *Prog. Energy Combust. Sci.*, 11, 119.